Ultrafast Interlayer Electron Transfer in Incommensurate Transition Metal Dichalcogenide Homo-bilayers

Yuanyuan Li,[†,‡] Qiannan Cui,[‡] Frank Ceballos,[‡] Samuel D. Lane,[‡] Zeming Qi,[*,†] and Hui Zhao[*,‡]

[†]*National Synchrotron Radiation Laboratory, University of Science and Technology of China, Hefei, Anhui, 230029, China*

[‡]*Department of Physics and Astronomy, The University of Kansas, Lawrence, Kansas 66045, United States*

E-mail: zmqi@ustc.edu.cn; huizhao@ku.edu

Phone: 1-785-864-1938

Abstract

Two-dimensional materials, such as graphene, transition metal dichalcogenides, and phosphorene, can be used to construct van der Waals multilayer structures. This approach has shown potentials to produce new materials that combine novel properties of the participating individual layers. One key requirement for effectively harnessing emergent properties of these materials is electronic connection of the involved atomic layers through efficient interlayer charge or energy transfer. Recently, ultrafast charge transfer on a time scale shorter than 100 fs has been observed in several van der Waals bilayer heterostructures formed by two different materials. However, information on the transfer between two atomic layers of the same type is rare. Since these homo-bilayers

are essential elements in constructing multilayer structures with desired optoelectronic properties, efficient interlayer is highly desired. Here we show that electron transfer between two monolayers of $MoSe_2$ occur on a picosecond time scale. Even faster transfer was observed in homo-bilayers of WS_2 and WSe_2. The samples were fabricated by manually stacking two exfoliated monolayer flakes. By adding a graphene layer as a fast carrier recombination channel for one of the two monolayers, the transfer of the photoexcited carriers from the populated to the drained monolayers was time-resolved by femtosecond transient absorption measurements. The observed efficient interlayer carrier transfer indicates that such homo-bilayers can be used in van der Waals multilayers to enhance their optical absorption without significantly compromising the interlayer transport performance. Our results also provide valuable information for understanding interlayer charge transfer in heterostructures.

KEYWORDS: van der Waals interface, transition metal dichalcogenide, electron transfer, transient absorption, two-dimensional material

Since the discovery of graphene in 2004,[1] two-dimensional (2D) materials have drawn considerable attention.[2–4] For example, transition metal dichalcogenides (TMDs) possess several exotic properties such as spin-valley coupling,[5–7] large exciton binding energy,[8,9] and strong nonlinear optical responses.[10–12] These properties indicate their potential applications in field-effect transistors,[13] integrated circuits,[14] solar cells,[15] photodetectors,[15] and light-emitting diodes.[16] In addition to their applications as individual materials, these monolayers (MLs) can also be used to form van der Waals multilayers heterostructures.[17] Comparing to conventional heterostructures formed by ionic or covalence materials, a significant advantage of this approach is the relaxation of the lattice mismatch requirement. As a result, many combinations of 2D materials can be explored to form new multilayer materials with tailored properties for targeted applications.

One key issue in harnessing emergent properties of van der Waals multilayers is to understand and control interlayer charge and energy transfer, which can effectively couple different

layers. Recent studies have indicated that interlayer charge transfer between two different TMD MLs occurs on an ultrafast time scale of shorter than 100 fs.[18–20] Although the detailed transfer mechanism is still under debate,[21–25] these results suggested the feasibility of constructing multilayer van der Waals materials with high interlayer transport performances. In contrast, however, studies on transfer across homo-interfaces formed by two TMD MLs of the same type are rare. When constructing van der Waals multilayers, twisted bilayers or few-layers of the same type can be important components, and efficient interlayer transfer is highly desired.

Twisted TMD bilayers have been used as a platform to study the mechanism of van der Waals interlayer coupling and its effects on the electronic structures. It has been revealed by photoluminescence (PL),[26,27] Raman spectroscopy,[26,27] and angular-resolved photoemission measurements[28] that for incommensurate MoS_2 bilayers with an arbitrary twist angle, significant interlayer coupling of the states near $\mathbf{\Gamma}$ point raises the top of the $\mathbf{\Gamma}$ valance band by more than 200 meV. The coupling is even stronger in commensurate bilayers, such as AA and AB-stacked bilayers, due to the smaller interlayer distance.[29] On the other hand, states in $\mathbf{K}$ valence band do not change significantly in bilayers compared to MLs[26–28] since the interlayer coupling of these states is suppressed by the giant spin-orbit coupling.[25] Consequently, the top of the $\mathbf{\Gamma}$ valance band is higher than $\mathbf{K}$, making bilayer MoS_2 an indirect semiconductor.[26,27,30]

So far, the effect of interlayer coupling on charge transfer is still yet to be understood. In TMD heterostructures, it was proposed that strong layer mixing in $\mathbf{\Gamma}$ and $\mathbf{Q}$ valleys can provide a fast interlayer charge transfer channel.[25] In homo-bilayers, however, electron transfer occurs between states with the same energy. Study of such interlayer transfer can thus provide new insight for understanding mechanisms of charge and energy transfer across van der Waals interfaces in general.

Here we report an experimental study on interlayer transfer in TMD homo-bilayers. Previously, time-resolved studies of interlayer charge transfer in van der Waals heterostructures

have utilized transient absorption measurements.[18–20] The key requirement of such measurements is to selectively excite and probe certain layers in a van der Waals multilayer, which was achieved by tuning the laser photon energies to the resonance of the targeted layers. This strategy requires that the layers forming heterostructures have different optical resonances,[18–20,31] which is often fulfilled in heterostructures. In homo-bilayers, however, both layers have the same resonance, which presents a significant challenge.

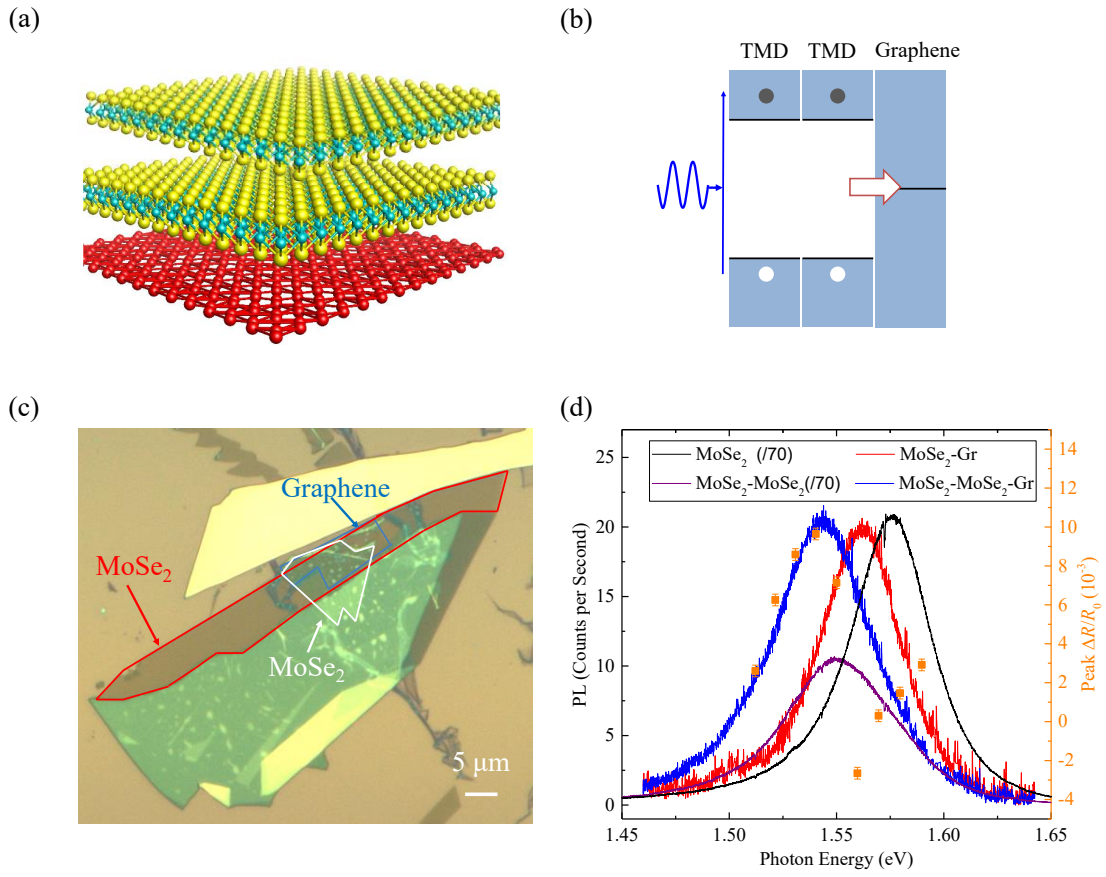

Figure 1: (a) Schematic illustration of the TMD-TMD-graphene samples. (b) The expected fast transfer of photocarriers across the TMD-graphene hetero-interface, leaving the left TMD the only populated layer. (c) Optical microscope image of a $MoSe_2$-$MoSe_2$-graphene sample. (d) Curves and left axis: Photoluminescence spectra of different regions of the sample. Gr stands for graphene. Symbols and right axis: peak differential reflection signal as a function of the probe photon energy measured from the trilayer region.

In our approach, we utilize a trilayer sample formed by two TMD MLs and a graphene ML, as schematically illustrated in Figure 1(a). Here, the graphene layer is used as a fast

recombination channel for the second TMD layer. Upon excitation of a laser pulse, photocarriers injected in the second TMD layer are expected to transfer to graphene [the horizontal arrow in Figure 1(b)] on a 100-fs time scale.[31] This process breaks the symmetric population of carriers among the two TMD layers, allowing time-resolved measurement of the transfer of photocarriers from the first to the second TMD layers. Once transferred, the photocarriers move to graphene quickly, and recombine. Hence, the decay of the population in the first $MoSe_2$ layer can provide information on the rate of this transfer across the TMD homojunction.

We studied interlayer transfer in incommensurate bilayers of $MoSe_2$, WSe_2, and WS_2, which were fabricated by mechanical exfoliation followed by a dry transfer process.[32] We will first focus on the $MoSe_2$-$MoSe_2$-graphene samples. Graphene flakes were first fabricated on Si/SiO_2 substrates. Monolayer regions were identified by their known optical contrast by using an optical microscope. Next, $MoSe_2$ flakes exfoliated from bulk crystals were transferred to polydimethylsiloxane (PDMS) substrates. Two identified ML flakes were then transferred on top of graphene sequentially. The $MoSe_2$ layers were purposely partially overlapped, so that the sample contains regions of $MoSe_2$ ML, $MoSe_2$-$MoSe_2$ bilayer, $MoSe_2$-graphene bilayer, as well as $MoSe_2$-$MoSe_2$-graphene trilayer. This facilitates direct comparison of these regions. Two samples with the same structure were studied. The results are similar. Here, we focus on the sample shown in Figure 1(c). The samples were under ambient condition at room temperature for all the measurements.

We first probed the quality of the interfaces and the effectiveness of interlayer transfer by PL spectroscopy. Figure 1(d) shows the PL spectra from different regions of the sample under the excitation of 1.96 eV and 8 μW. The $MoSe_2$ ML region shows strong PL of about 1400 counts per second, centered at 1.573 eV (black curve). In the $MoSe_2$-graphene region, the PL intensity is quenched by about a factor of 70 (red curve). This indicates that the majority of the photocarriers injected in $MoSe_2$ transfer to graphene efficiently, instead of recombining radiatively in $MoSe_2$. The $MoSe_2$-$MoSe_2$ bilayer region shows a PL intensity

of about half, instead of twice, of the ML PL (purple curve). This indicates the effect of interlayer coupling on the band structure and photocarrier dynamics.[26,27,33] The PL of the trilayer region (blue curve) shows similar intensity as the $MoSe_2$-graphene region. This indicates that the photocarriers injected in the first $MoSe_2$ can effectively transfer to the other two layers, before their radiative recombination.

It is interesting to note that the PL peak shifts to lower energy side as the layer number increases. The peak energies of the $MoSe_2$-graphene and $MoSe_2$-$MoSe_2$ bilayer regions are more than 10 meV lower than the ML region. In the trilayer region, the peak is further shifted to 1.543 eV, which is 30-meV lower than the peak energy in the ML region. We attribute the shift to the change of the optical bandgap of $MoSe_2$ by the screening effect of the adjacent layers. It has been recognized that the electron-electron interaction and electron-hole interaction in MLs can be significantly screened by adjacent layers, since a significant portion of the electric field lines extends out of the ML.[8] The larger shift in the trilayer observed is consistent with this interpretation, where the field is screened by two layers instead of one.

The interlayer transfer was time resolved by transient absorption measurements. In such measurements, a pump pulse was used to inject photocarriers in the sample. The dynamics of the carriers were detected by measuring differential reflection of a probe pulse. The differential reflection is defined as $\Delta R/R_0 = (R - R_0)/R_0$, where R and R_0 are the reflectivity of the probe with and without the presence of the pump, respectively. In the low-density regime, the differential reflection is approximately proportional to the carrier density. Hence, by measuring it as a function of the delay of the probe pulse with respect to the arrival time of the pump pulse, called probe delay, the evolution of the carrier density can be time resolved.[34]

We first measured the $MoSe_2$ ML region with a pump of 1.907 eV and a probe of 1.540 eV, which is near the A-exciton resonance. The normalized differential reflection signal is shown as the black symbols in Figure 2. A single-exponential function with a baseline,

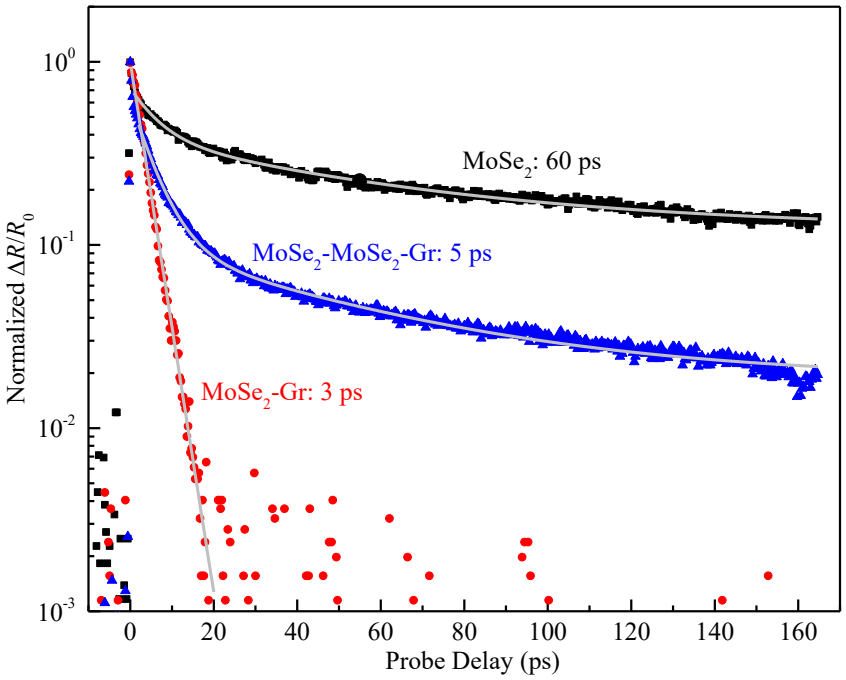

Figure 2: Normalized differential reflection signal from $MoSe_2$ monolayer (black), $MoSe_2$-graphene bilayer (red), and $MoSe_2$-$MoSe_2$-graphene trilayer (blue). The gray curves are fits (see text).

$\Delta R/R_0 = Ae^{-t/\tau} + B$, was used to fit the decay of the signal, which yielded a time constant of $\tau = 60$ ps. The baseline (B) is included in order to account for the long-lived (nanoseconds) signal. This component is about 20% of the peak signal, and could be due to thermal effect or from trapped carriers. Nevertheless, this slow-varying component does not affect the measurement of the photocarrier lifetime in $MoSe_2$ ML of about 60 ps. We next repeated the measurement in the $MoSe_2$-graphene bilayer region. The signal decays rapidly (red symbols), with a decay constant of 3 ps. Previously, we have shown that in TMD-graphene bilayers, the carriers injected in TMD transfer to graphene on a time scale shorter than 100 fs,[31] and that the transient absorption signal at TMD exciton resonance is dominated by the transferred carriers in graphene, due to the strong screening effect.[31] Hence, the 3-ps decay time is attributed to photocarrier lifetime in graphene.

The blue symbols in Figure 2 show the result of the same measurement performed in the trilayer region. Clearly, the decay of the signal is faster than the ML region, but slower than

the $MoSe_2$-graphene bilayer. A bi-exponential fit, $\Delta R/R_0 = A_1 e^{-t/\tau_1} + A_2 e^{-t/\tau_2} + B$, to the data after 1 ps yields a fast time constant of $\tau_1 = 5$ ps and a slow time constant of $\tau_2 = 65$ ps. The measurement was repeated with various probe photon energies. The peak signal shows a strong dependence on the probe photon energy, as shown by the orange symbols in Figure 1(d), while the temporal evolution is independent of it.

The comparison of $MoSe_2$ ML, $MoSe_2$-graphene bilayer, and $MoSe_2$-$MoSe_2$-graphene trilayer regions shows clearly the effect of the photocarrier transfer between the two $MoSe_2$ MLs. Without efficient transfer, the decay of the signal from the trilayer sample would be dominated by recombination of carriers in the first $MoSe_2$ layer, on a time scale of 60 ps. Based on our observations and recent reports on TMD bilayers, we propose the transfer mechanism as illustrated in Figure 3. Potential contributions from energy transfer will be discussed in a later paragraph. After photoexcitation [blue vertical arrow in (a)] across the direct bandgap in **K** valleys (orange curves), the electrons (black circle) and holes (white circle) excited in the second $MoSe_2$ layer transfer to graphene on an ultrafast time scale of shorter than 100 fs (green arrows).[31] The holes excited in **K** valley of the first $MoSe_2$ layer relax to $\mathbf{\Gamma}$ valley through efficient phonon-assisted intervalley scattering.[25] Due to interlayer mixing, the hole wavefunction extends to both $MoSe_2$ layers, facilitating its transfer to graphene. Since all the transfer processes described above occurs on 100-fs time scale or shorter, after the excitation of the pump pulse of about 150 fs, we expect the system to arrive at a state shown in Figure 3(b). The rest of dynamics is controlled by recombination of carriers in graphene (3 ps) and transfer of electrons from the first to the second $MoSe_2$ layer (followed by a rapid transfer to graphene). Hence, the decay time of 5 ps in trilayer indicates that the interlayer transfer of electrons is a picosecond process. The transfer of electrons is driven by the Coulomb field from the graphene layer, which is positively charged with excess holes [Figure 3(b)].

The picosecond interlayer transfer time deduced is much longer than previous observed charge transfer times (< 100 fs) in TMD heterostructures.[18–20] In a heterostructure, electrons

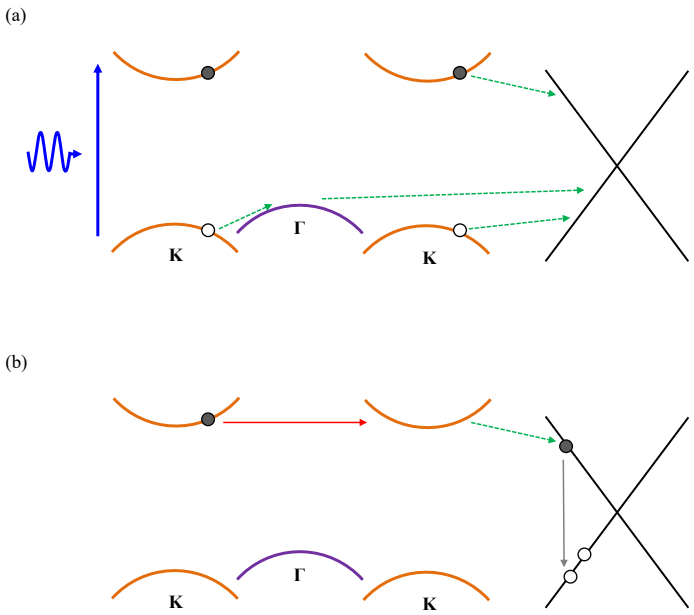

Figure 3: Schematic illustration of carrier dynamics. (a) Pump pulse injects electron-hole pairs in **K** valley of both $MoSe_2$ layers. Carriers excited in the second layer transfer to graphene rapidly. Holes in **K** valley of the first layer relax to the layer-coupled **Γ** valley, and subsequently transfer to graphene. (b) After the ultrafast processes illustrated by the green arrows in (a), electrons in **K** valley of the first layer transfer to second layer, driven by the Coulomb force from the holes, and then rapidly transfer to graphene. Finally, recombination of carriers in graphene brings the system to the ground state.

excited in the layer of higher **K** valley can quickly transfer to the layer of lower **K** valley *via* intervalley scattering to the layer-coupled **Q** valley.[25] This process is allowed and efficient because the **Q** valley has lower energy than the higher **K** valley.[25] However, in $MoSe_2$, it has been shown that even in commensurate bilayers, the interlayer coupling is not sufficient to bring the **Q** valley below **K**.[35] In this case, the electrons in **K** valley do not have enough energy to transfer to **Q** valley. Hence, the observed slower electron transfer between two $MoSe_2$ layers supports the fast charge transfer mechanism *via* layer-coupled states. We note that although the twist angle between the two $MoSe_2$ layers are unknown in our samples, the observed interlayer transfer is expected to be independent of the twist angle for two reasons. First, the interlayer coupling is only weakly dependent on the twist angle for incommensurate bilayers.[25–27] Second, the transfer is limited by the electron transfer between **K** valleys that are nearly uncoupled.

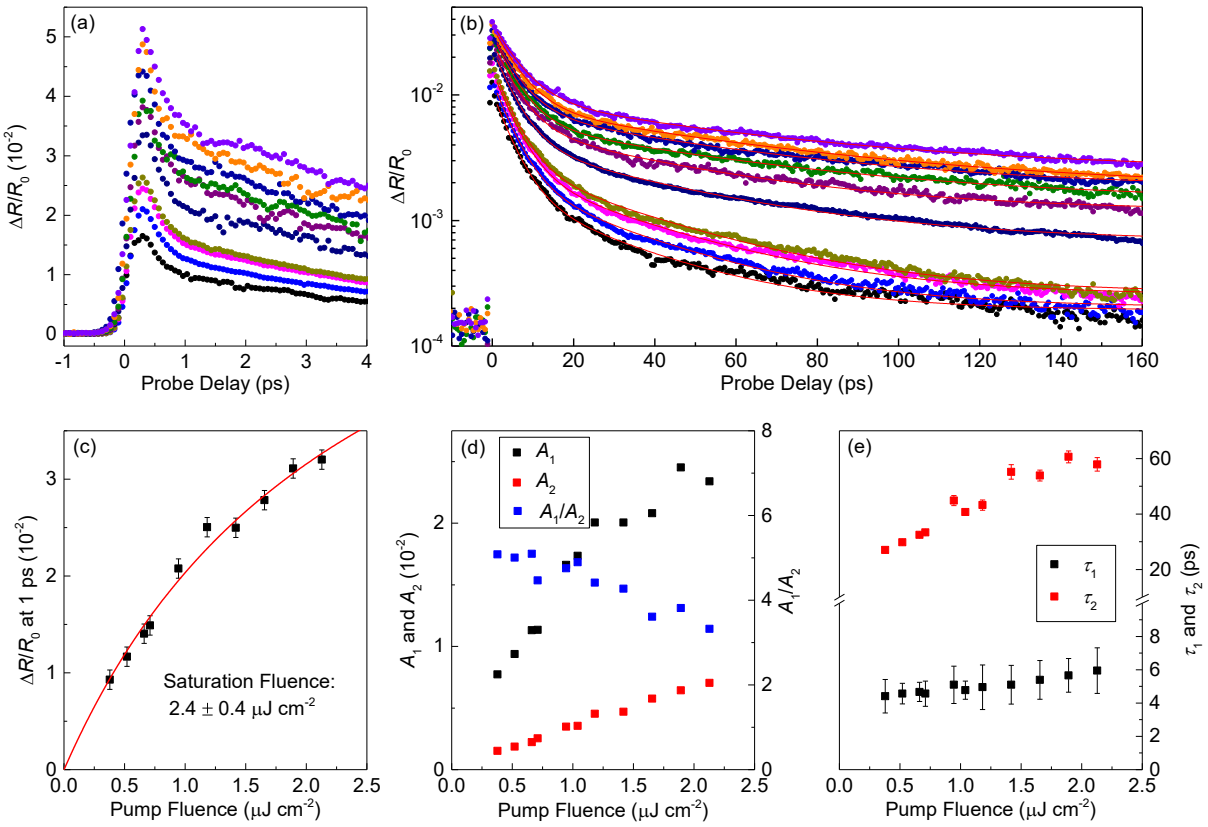

Figure 4: Differential reflection signal from the $MoSe_2$-$MoSe_2$-graphene sample with different values of pump fluence in short (a) and long (b) time ranges. The decay of the signal was fit by bi-exponential functions (red curves). (c) shows the signal at 1 ps as a function of pump fluence. The amplitudes and time constants from the fits are summarized in (d) and (e).

To gain more insight about the carrier dynamics, we performed a measurement of this process with different values of pump fluence. Figure 4 shows the differential reflection of a 1.57-eV probe measured from the trilayer sample with different values of the energy fluence of the 1.907-eV pump pulse. Different curves in (a) and (b) correspond to different values of pump fluence in the range of 0.5 (bottom) to 2.5 μJ cm^{-2} (top). From the absorption coefficient of $MoSe_2$ ML[36] and graphene[37] for 1.907 eV, we estimate that a pump pulse of 1 μJ cm^{-2} injects an areal density of about 5 $\times$ 10^{10} cm^{-2} in each $MoSe_2$ layer, and about 1 $\times$ 10^{10} cm^{-2} in graphene. The initial sub-ps decay of the signal could be attributed to exciton formation.[38,39] Figure 4(c) shows the dependence of the signal at 1 ps (after this transient process) as a function of the pump fluence, which can be fit by a saturation

model, $\Delta R/R_0 \propto F/(F + F_{sat})$, with a saturation fluence of $F_{sat} = 2.4 \pm 0.4$ μJ cm^{-2}. This corresponds to a saturation density of about 1.2×10^{11} cm^{-2}. At low densities, the signal is approximately proportional to the carrier density. This justifies deduction of carrier dynamics by analyzing the time evolution of the signal. The decay of the signal after 1 ps (*i.e.* after the exciton formation process) was fit by the bi-exponential function mentioned above, as shown by the curves in Figure 4(b), with the fitting parameters summarized in (d) and (e). The fast-decay component (A_1) accounts for about 80% of the signal, as A_1/A_2 is about 5 at low densities [blue symbols in (d)]. The corresponding time constant τ_1 is in the range of 5 - 6 ps, only weakly depends on the pump fluence [black symbols in (e)].

The long time constant in the range of 30 - 60 ps can be attributed to recombination of photocarriers that do not transfer to graphene, which are excited in the regions with relatively poor interfacial contact. It was known that interfacial contaminations tend to form bubbles during thermal annealing process,[40] as can be seen in Figure 1(c). The bubbles separate the two layers, preventing effective interlayer coupling and transfer between the two $MoSe_2$ layers or between the second $MoSe_2$ layer and graphene. In the regions with bubbles, the decay of the signal is expected to be similar to $MoSe_2$ ML, due to lack of interlayer coupling. In the measurements, if part of the sample excited by the laser spot contains such contamination, carriers excited in these regions would produce a long-lived signal, as we observed. However, measurement of interlayer transfer is based on the short-lived signal from regions with high quality interface, and is not influenced by these contaminations. This interpretation is further supported by the observation that the ratio of the two components varies in a random fashion among different samples studied, while the time constants are very consistent (see Supporting Information). It is also interesting to note that the lifetime increases with density, which is opposite to what one would expect from exciton-exciton annihilation.[41,42] The reason is unclear to us. However, since this feature originates from parts of the sample with poor interface quality and occurs on a time scale much longer than transfer time, it does not impact our discussions on interlayer transfer.

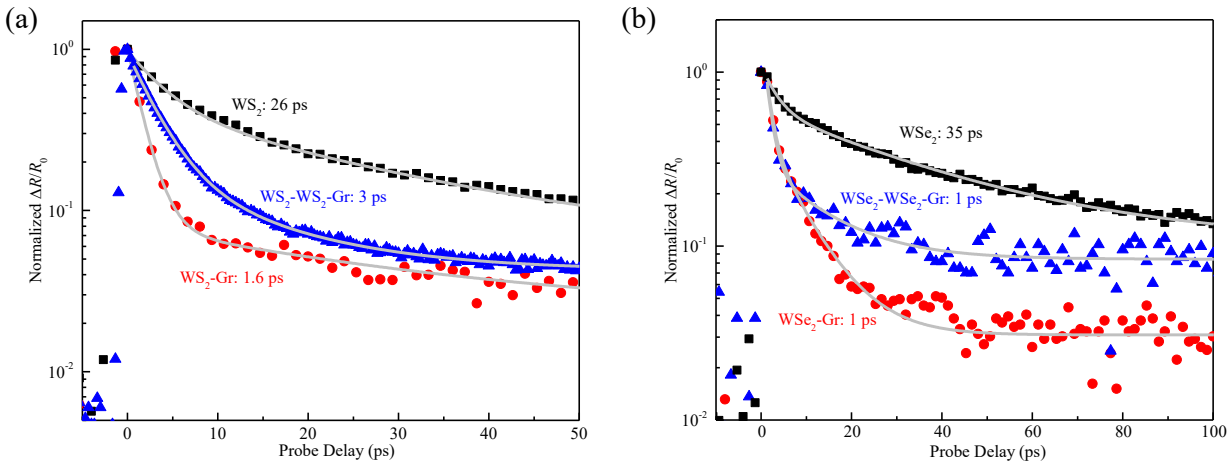

Figure 5: (a) Normalized differential reflection signal from a WS_2 monolayer (black), a WS_2-graphene bilayer (red), and a WS_2-WS_2-graphene trilayer (blue). The samples were pumped with 3.10-eV and probed with 2.00-eV photons. The light gray curves are exponential fits. (b) Same as (a), but for WSe_2-based samples. The pump and probe photon energies are 3.10 and 1.68 eV, respectively.

We also studied two other sets of samples based on WS_2 and WSe_2. Figure 5(a) shows results of WS_2-based samples. The signal from WS_2 ML decays exponentially with a time constant of 26 ps. The WS_2-graphene bilayer showed a rapid decay of 1.6 ps, while the WS_2-WS_2-graphene trilayer yielded a decay time of 3 ps. The results also indicate picosecond interlayer carrier transfer between the two randomly stacked WS_2 layers. A similar power-dependent measurement, as shown in Figure 4, was performed, too. The results are provided in Supporting Information. Finally, in WSe_2 samples, the decay of the signals from WSe_2-WSe_2-graphene and WSe_2-graphene are both about 1 ps, which is much shorter than WSe_2 ML (35 ps), as shown in Figure 5(b) (details on power-dependence are given in Supporting Information). The results suggest the interlayer carrier transfer between WSe_2 occurs on a much shorter (sub-picosecond) time scale. This could suggest that the charge transfer channel via layer-coupled states is also available for electrons in WSe_2 bilayers. Indeed, this is consistent with calculated bandstructures, which show that the **Q** valley in bilayer WSe_2 is lower than **K** valley.[43,44]

Finally, we note that if only the initial and final states of the process studied here are

considered, the process mimics Dexter energy transfer:[45,46] Both the electrons and the holes excited in the first TMD layer eventually transfer to graphene, without a net charge transfer. Our interpretation of the transfer mechanism is based on efficient transfer of holes *via* strongly-coupled states in $\mathbf{\Gamma}$ valley, as illustrated in Figure 3. A recent paper showed that Förster-type energy transfer occurs in a TMD heterostructure with a time scale of about 1 ps.[47] Hence, it is interesting to estimate potential contributions of Förster energy transfer to the observed dynamics. The potential transfers are TMD1 to TMD2, TMD1 to graphene, and TMD2 to graphene, where TMD1 and TMD2 are the first and second TMD layers in the trilayers. The TMD2-to-graphene process has been established as a 100-fs process through our previous studies[31] and is further confirmed here (rising of signals from TMD-graphene bilayers). Since the TMD1-to-TMD2 process is a 1-ps process, TMD1-to-graphene is expected to be slower by at least several times due to the larger separation of the two layers, as the transfer rate rapidly decreases with increasing the distance.[47,48] If the 100-fs charge transfer channeling is available, as suggested by previous studies on heterostructures,[18–20] the TMD1-to-TMD2 and TMD1-to-graphene Förster transfer processes are expected to play minor roles in the decay of carrier population in TMD1, since once the holes transferred, the electrons cannot recombine for energy transfer. On the other hand, if the fast charge-transfer channel is not available in TMD homo-bilayers, the decay of the population in the first TMD layer would be dominated by TMD1-to-TMD2 Förster transfer followed by the 100-fs TMD2-to-graphene transfer, since this process is expected to be at least several times faster than the TMD1-to-graphene process. Based on these arguments, our experimental conclusion on the picosecond transfer time in TMD homo-bilayers does not rely on the availability of the charge-transfer channels, although the transfer mechanism does.

In summary, by using a graphene layer as a fast-recombination channel, we have time-resolved, for the first time, transfer of photocarriers between two randomly stacked TMD MLs of the same type. We found that the transfer between two $MoSe_2$ and two WS_2 layers occurs on a picosecond time scale, or with a transfer rate on the order of 10^{12} s^{-1}. Even faster (and

non-resolvable) transfer was observed between WSe_2 layers. The efficient interlayer transfer between randomly stacked and incommensurate TMD MLs indicates that such homo-bilayers can be used as building blocks for van der Waals multilayers to achieve desired optical thicknesses without scarifying interlayer transport performances. These results also provide information for understanding charge and energy transfer across different types of van der Waals interfaces.

Acknowledgments

This material is based upon work supported by the National Science Foundation of USA (No. DMR-1505852), National Natural Science Foundation of China (No. 11275203), and Technological Development Grant of Hefei Science Center of CAS (2014TDG-HSC002). SDL acknowledges financial support of Madison & Lila Self Graduate Fellowship.

Supporting Information Available

The following files are available free of charge.

Additional figures on WS_2-WS_2-graphene and WSe_2-WSe_2-graphene samples.

References

(1) Novoselov, K. S.; Geim, A. K.; Morozov, S. V.; Jiang, D.; Zhang, Y.; Dubonos, S. V.; Grigorieva, I. V.; Firsov, A. A. *Science* **2004**, *306*, 666–669.

(2) Gibney, E. *Nature* **2015**, *522*, 274–276.

(3) Neto, A. H. C.; Novoselov, K. *Rep. Prog. Phys.* **2011**, *74*, 082501.

(4) Wang, Q. H.; Kalantar-Zadeh, K.; Kis, A.; Coleman, J. N.; Strano, M. S. *Nat. Nanotechnol.* **2012**, *7*, 699–712.

(5) Xiao, D.; Liu, G. B.; Feng, W.; Xu, X.; Yao, W. *Phys. Rev. Lett.* **2012**, *108*, 196802.

(6) Zeng, H.; Dai, J.; Yao, W.; Xiao, D.; Cui, X. *Nat. Nanotechnol.* **2012**, *7*, 490–493.

(7) Mak, K. F.; He, K.; Shan, J.; Heinz, T. F. *Nat. Nanotechnol.* **2012**, *7*, 494–498.

(8) Chernikov, A.; Berkelbach, T. C.; Hill, H. M.; Rigosi, A.; Li, Y. L.; Aslan, O. B.; Reichman, D. R.; Hybertsen, M. S.; Heinz, T. F. *Phys. Rev. Lett.* **2014**, *113*, 076802.

(9) He, K.; Kumar, N.; Zhao, L.; Wang, Z.; Mak, K. F.; Zhao, H.; Shan, J. *Phys. Rev. Lett.* **2014**, *113*, 026803.

(10) Kumar, N.; Najmaei, S.; Cui, Q.; Ceballos, F.; Ajayan, P. M.; Lou, J.; Zhao, H. *Phys. Rev. B* **2013**, *87*, 161403.

(11) Malard, L. M.; Alencar, T. V.; Barboza, A. P. M.; Mak, K. F.; de Paula, A. M. *Phys. Rev. B* **2013**, *87*, 201401.

(12) Li, Y.; Rao, Y.; Mak, K. F.; You, Y.; Wang, S.; Dean, C. R.; Heinz, T. F. *Nano Lett.* **2013**, *13*, 3329–3333.

(13) Radisavljevic, B.; Radenovic, A.; Brivio, J.; Giacometti, V.; Kis, A. *Nat. Nanotechnol.* **2011**, *6*, 147–150.

(14) Wang, H.; Yu, L. L.; Lee, Y. H.; Shi, Y. M.; Hsu, A.; Chin, M. L.; Li, L. J.; Dubey, M.; Kong, J.; Palacios, T. *Nano Lett.* **2012**, *12*, 4674–4680.

(15) Baugher, B. W. H.; Churchill, H. O. H.; Yang, Y.; Jarillo-Herrero, P. *Nat. Nanotechnol.* **2014**, *9*, 262–267.

(16) Zhang, Y. J.; Oka, T.; Suzuki, R.; Ye, J. T.; Iwasa, Y. *Science* **2014**, *344*, 725–728.

(17) Geim, A. K.; Grigorieva, I. V. *Nature* **2013**, *499*, 419–425.

(18) Hong, X.; Kim, J.; Shi, S. F.; Zhang, Y.; Jin, C.; Sun, Y.; Tongay, S.; Wu, J.; Zhang, Y.; Wang, F. *Nat. Nanotechnol.* **2014**, *9*, 682–686.

(19) Ceballos, F.; Bellus, M. Z.; Chiu, H. Y.; Zhao, H. *ACS Nano* **2014**, *8*, 12717–12724.

(20) Peng, B.; Yu, G.; Liu, X.; Liu, B.; Liang, X.; Bi, L.; Deng, L.; Sum, T. C.; Loh, K. P. *2D Mater.* **2016**, *3*, 025020.

(21) Zhu, X.; Monahan, N. R.; Gong, Z.; Zhu, H.; Williams, K. W.; Nelson, C. A. *J. Am. Chem. Soc.* **2015**, *137*, 8313–8320.

(22) Long, R.; Prezhdo, O. V. *Nano Lett.* **2016**, *16*, 1996–2003.

(23) Wang, H.; Bang, J.; Sun, Y. Y.; Liang, L. B.; West, D.; Meunier, V.; Zhang, S. B. *Nat. Commun.* **2016**, *7*, 11504.

(24) Ceballos, F.; Ju, M. G.; Lane, S. D.; Zeng, X. C.; Zhao, H. *Nano Lett.* **2017**, *17*, 1623–1628.

(25) Wang, Y.; Wang, Z.; Yao, W.; Liu, G. B.; Yu, H. Y. *Phys. Rev. B* **2017**, *95*, 115429.

(26) Liu, K.; Zhang, L.; Cao, T.; Jin, C.; Qiu, D.; Zhou, Q.; Zettl, A.; Yang, P.; Louie, S. G.; Wang, F. *Nat. Commun.* **2014**, *5*, 4966.

(27) van der Zande, A. M.; Kunstmann, J.; Chernikov, A.; Chenet, D. A.; You, Y.; Zhang, X.; Huang, P. Y.; Berkelbach, T. C.; Wang, L.; Zhang, F.; Hybertsen, M. S.; Muller, D. A.; Reichman, D. R.; Heinz, T. F.; Hone, J. C. *Nano Lett.* **2014**, *14*, 3869–3875.

(28) Yeh, P. C.; Jin, W.; Zaki, N.; Kunstmann, J.; Chenet, D.; Arefe, G.; Sadowski, J. T.; Dadap, J. I.; Sutter, P.; Hone, J.; Osgood, R. M. *Nano Lett.* **2016**, *16*, 953–959.

(29) Huang, S.; Ling, X.; Liang, L.; Kong, J.; Terrones, H.; Meunier, V.; Dresselhaus, M. S. *Nano Lett.* **2014**, *14*, 5500–5508.

(30) He, J. G.; Hummer, K.; Franchini, C. *Phys. Rev. B* **2014**, *89*, 075409.

(31) He, J.; Kumar, N.; Bellus, M. Z.; Chiu, H. Y.; He, D.; Wang, Y.; Zhao, H. *Nat. Commun.* **2014**, *5*, 5622.

(32) Bellus, M. Z.; Ceballos, F.; Chiu, H.-Y.; Zhao, H. *ACS Nano* **2015**, *9*, 6459–6464.

(33) Zheng, S. J.; Sun, L. F.; Zhou, X. H.; Liu, F. C.; Liu, Z.; Shen, Z. X.; Fan, H. J. *Adv. Opt. Mater.* **2015**, *3*, 1600–1605.

(34) Ceballos, F.; Zhao, H. *Adv. Funct. Mater.* **2017**, *27*, 1604509.

(35) Zhang, Y. et al. *Nat. Nanotechnol.* **2014**, *9*, 111–115.

(36) Liu, H.-L.; Shen, C.-C.; Su, S.-H.; Hsu, C.-L.; Li, M.-Y.; Li, L.-J. *Appl. Phys. Lett.* **2014**, *105*, 201905.

(37) Mak, K. F.; Sfeir, M. Y.; Wu, Y.; Lui, C. H.; Misewich, J. A.; Heinz, T. F. *Phys. Rev. Lett.* **2008**, *101*, 196405.

(38) Ceballos, F.; Cui, Q.; Bellus, M. Z.; Zhao, H. *Nanoscale* **2016**, *8*, 11681–11688.

(39) Steinleitner, P.; Merkl, P.; Nagler, P.; Mornhinweg, J.; Schuller, C.; Korn, T.; Chernikov, A.; Huber, R. *Nano Lett.* **2017**, *17*, 1455–1460.

(40) Haigh, S. J.; Gholinia, A.; Jalil, R.; Romani, S.; Britnell, L.; Elias, D. C.; Novoselov, K. S.; Ponomarenko, L. A.; Geim, A. K.; Gorbachev, R. *Nat. Mater.* **2012**, *11*, 764–767.

(41) Sun, D.; Rao, Y.; Reider, G. A.; Chen, G.; You, Y.; Brezin, L.; Harutyunyan, A. R.; Heinz, T. F. *Nano Lett.* **2014**, *14*, 5625–5629.

(42) Kumar, N.; Cui, Q.; Ceballos, F.; He, D.; Wang, Y.; Zhao, H. *Phys. Rev. B* **2014**, *89*, 125427.

(43) Sahin, H.; Tongay, S.; Horzum, S.; Fan, W.; Zhou, J.; Li, J.; Wu, J.; Peeters, F. M. *Phys. Rev. B* **2013**, *87*, 165409.

(44) Zhao, W. J.; Ribeiro, R. M.; Toh, M. L.; Carvalho, A.; Kloc, C.; Neto, A. H. C.; Eda, G. *Nano Lett.* **2013**, *13*, 5627.

(45) Dexter, D. L. *J. Chem. Phys.* **1953**, *21*, 836–850.

(46) Murphy, C. B.; Zhang, Y.; Troxler, T.; Ferry, V.; Martin, J. J.; Jones, W. E. *J. Phys. Chem. B* **2004**, *108*, 1537–1543.

(47) Kozawa, D.; Carvalho, A.; Verzhbitskiy, I.; Giustiniano, F.; Miyauchi, Y.; Mouri, S.; Neto, A. H. C.; Matsuda, K.; Eda, G. *Nano Lett.* **2016**, *16*, 4087–4093.

(48) Rigos, A. F.; Hill, H. M.; Li, Y. L.; Chernikov, A.; Heinz, T. F. *Nano Lett.* **2015**, *15*, 5033–5038.